INTERNATIONAL JOURNAL FOR NUMERICAL METHODS IN FLUIDS
Int. J. Numer. Meth. Fluids 2002; **39**:639–656 (DOI: 10.1002/fld.351)

A multi-dimensional monotonic finite element model for solving the convection–diffusion-reaction equation

Tony W. H. Sheu*,† and Harry Y. H. Chen

Department of Engineering Science and Ocean Engineering, National Taiwan University, 73 Chou-Shan Rd., Taipei, Taiwan, Republic of China

SUMMARY

In this paper, we develop a finite element model for solving the convection–diffusion-reaction equation in two dimensions with an aim to enhance the scheme stability without compromising consistency. Reducing errors of false diffusion type is achieved by adding an artificial term to get rid of three leading mixed derivative terms in the Petrov–Galerkin formulation. The finite element model of the Petrov–Galerkin type, while maintaining convective stability, is modified to suppress oscillations about the sharp layer by employing the M-matrix theory. To validate this monotonic model, we consider test problems which are amenable to analytic solutions. Good agreement is obtained with both one- and two-dimensional problems, thus validating the method. Other problems suitable for benchmarking the proposed model are also investigated. Copyright © 2002 John Wiley & Sons, Ltd.

KEY WORDS: convection–diffusion-reaction equation; two dimensions; Petrov–Galerkin formulation; M-matrix theory; monotonic

1. INTRODUCTION

The scalar convection–diffusion-reaction (CDR) equation is examined as a linear model for simulating time-dependent equations in areas of fluid dynamics and heat transfer. In addition, this equation is practically important, as it is akin to the constitutive equations used to model the transport of turbulent kinetic energy and its dissipation [1]. In addition, constitutive equations for the extra stress tensor in viscoelastic fluid flows fall into this category [2]. In an externally applied magnetic field, the magnetic induction equation for liquid metals is classified as the CDR equation as well [3]. The Helmholtz equation, a special form of CDR equation, governs wave propagation in areas of exterior and fibre acoustics [4]. It is this wide application scope that makes numerical investigation of CDR equation worthwhile.

* Correspondence to: Tony W. H. Sheu, Department of Engineering Science & Ocean Engineering, National Taiwan University, 73 Chou-Shan Road, Taipei, Taiwan, Republic of China.
† E-mail: sheu@sccs.na.ntu.edu.tw

Contract/sponsor: National Science Council; contract/grant number: NSC88-2611-E-002-025.

Received August 2001
Revised October 2001

Compared with the considerable amount of effort that has been invested in developing the convection–diffusion schemes, fewer studies have been devoted to the more general CDR equation [5–11] and the development of discontinuity-capturing CDR schemes [12–14]. A reliable CDR model must have the ability to render accurate solutions while suppressing numerical oscillations of different kinds. The problem of numerical instability stems from the occurrence of convection and reaction terms. It is, therefore, necessary to construct stabilization schemes, and this motivated the present study. In this paper, we are also concerned with prediction accuracy since we do not regard a scheme as useful if it cannot provide accuracy to a certain high level in the computation of two-dimensional problems. Another goal in the present model development is to resolve field variables in the vicinity of sharp layers.

The rest of this paper is organized as follows. Section 2 presents the working equation. This is followed by presentation of the one-dimensional finite element model. The essential elements of the proposed model are then presented in greater detail in Section 4. Our emphasis is on obtaining results that are less contaminated by false diffusion errors and on obtaining oscillation-free solutions in the vicinity of sharp layers. Section 5 presents numerical results that can demonstrate the validity of the method. In Section 6, we give concluding remarks.

2. WORKING EQUATIONS

The following CDR equation is often considered as the model equation for schemes developed to solve the fluid dynamics and heat transfer problems:

$$\phi_t + \bar{u}\phi_x + \bar{v}\phi_y - \bar{\mu}(\phi_{xx} + \phi_{yy}) + \bar{R}\phi = 0 \tag{1}$$

In the above, $\bar{u}$ and $\bar{v}$ represent the velocity components along the x and y directions, respectively. Other coefficients involve $\bar{\mu}$ and $\bar{R}$, which denote the diffusion (or fluid viscosity) and the reaction coefficient, respectively. By conducting the Euler implicit time-stepping scheme on ϕ_t, we can obtain the steady-state CDR equation $u\phi_x + v\phi_y - \mu(\phi_{xx} + \phi_{yy}) + R\phi = f$, where $u = \bar{u}\Delta t$, $v = \bar{v}\Delta t$, $R = (1 + \bar{R}\Delta t)$ and $f = \phi^n$. It is, therefore, instructive to analyse the following model equation:

$$u\phi_x + v\phi_y - \mu(\phi_{xx} + \phi_{yy}) + R\phi = f \tag{2}$$

We shall, for illustrative purposes, assume that (u, v), μ, and R are constant throughout. For simplicity, the value of ϕ is sought subject to $\phi = g$ on the boundary $\partial\Omega$.

3. FINITE ELEMENT MODEL

Like other numerical methods, the finite element method has a sound mathematical basis for proving the convergence of solutions. Apart from this theoretical foundation, the finite element method is favourably used when solving problems involving complex geometry. Within the weighted residual framework, the finite element solution for Equation (2) is computed using $\int W_i(\underline{u} \cdot \nabla\phi - \mu\nabla^2\phi + R\phi)\,\mathrm{d}\Omega = \int W_i f\,\mathrm{d}\Omega$. The key to obtaining highly accurate solutions exhibiting the non-oscillatory property lies in choosing an appropriate weighting function W_i. We shall, in what follows, address the construction of W_i in the linear element context.

To simplify matters in the case of high Peclet, we will first derive W_i based on the following one-dimensional CDR equation:

$$u\nabla\phi - \mu\nabla^2\phi + R\phi = f \tag{3}$$

The Galerkin representation of Equation (3) in a linear element $\Omega_e = \{x_i, x_{i+1}\}$ takes the following matrix form:

$$\begin{bmatrix} \frac{-uh}{2} & \frac{uh}{2} \\ \frac{-uh}{2} & \frac{uh}{2} \end{bmatrix} \begin{bmatrix} \phi_i \\ \phi_{i+1} \end{bmatrix} + \begin{bmatrix} \frac{\mu}{h^2} & \frac{-\mu}{h^2} \\ \frac{-\mu}{h^2} & \frac{\mu}{h^2} \end{bmatrix} \begin{bmatrix} \phi_i \\ \phi_{i+1} \end{bmatrix} + \begin{bmatrix} \frac{R}{3} & \frac{R}{6} \\ \frac{R}{6} & \frac{R}{3} \end{bmatrix} \begin{bmatrix} \phi_i \\ \phi_{i+1} \end{bmatrix} = \begin{bmatrix} \frac{1}{3} & \frac{1}{6} \\ \frac{1}{6} & \frac{1}{3} \end{bmatrix} \begin{bmatrix} f_i \\ f_{i+1} \end{bmatrix} \tag{4}$$

In the above, $h(\equiv x_{i+1} - x_i)$ denotes the grid size. The assemblage of two elements having the nodal point i in common results in the finite element equation for ϕ_i

$$\left(\frac{-u}{2h} - \frac{\mu}{h^2} + \frac{R}{6}\right)\phi_{i-1} + \left(\frac{2\mu}{h^2} + \frac{2R}{3}\right)\phi_i + \left(\frac{u}{2h} - \frac{\mu}{h^2} + \frac{R}{6}\right)\phi_{i+1} = \frac{1}{6}f_{i-1} + \frac{2}{3}f_i + \frac{1}{6}f_{i+1} \tag{5}$$

Equation (5) shows that the dominance of the matrix diagonal decreases as the reaction coefficient decreases and the velocity $|u|$ increases. As the accompanying instabilities are numerical in origin, refinement of W_i from the shape function N_i is warranted. In keeping with the above, W_i $(i = 1, 2)$ is expressed as follows:

$$W_i = N_i + \tau u \frac{\partial N_i}{\partial x} + P_i \tag{6}$$

The last two terms are introduced for stabilizing the scheme applied in the case of high Peclet number R_1

$$R_1 = \frac{uh}{\mu} \tag{7}$$

and low reaction number R_2

$$R_2 = \frac{Rh^2}{\mu} \tag{8}$$

Substituting (6) into Equation (2), the linear finite element equation at an arbitrary point i is derived from

$$\int_\Omega \left(N_i + \tau u \frac{\partial N_i}{\partial x} + P_i\right)(u\nabla\phi - \mu\nabla^2\phi + R\phi - f)\,\mathrm{d}\Omega = 0 \tag{9}$$

As our goal is to enhance Galerkin formulation, we need to refine the third matrix in Equation (4) by introducing parameters δ and λ. One can change

$$\frac{R}{3}\begin{bmatrix} 1 & \frac{1}{2} \\ \frac{1}{2} & 1 \end{bmatrix}$$

to

$$\frac{R}{3}\begin{bmatrix} \delta & \lambda \\ \lambda & \delta \end{bmatrix}$$

by choosing P_1 and P_2 as

$$P_1 = \tfrac{1}{6}(-3 + 2\delta + \lambda) + \tfrac{1}{2}(1 - 2\delta + \lambda)\xi \tag{10}$$

$$P_2 = \tfrac{1}{6}(-3 + 2\delta + \lambda) - \tfrac{1}{2}(1 - 2\delta + \lambda)\xi \tag{11}$$

where $-1 \leqslant \xi \leqslant 1$ denotes the master co-ordinate. After some algebra, the following modified equation [15] for (9):

$$u\phi_x - \mu u_{xx} + R\phi - f = Ru\tau\phi_x + \left[\mu\frac{4(\delta-\lambda)}{3} + u^2\tau - \frac{\lambda h^2 R}{6}\right]\phi_{xx} + \text{H.O.T.} \tag{12}$$

is derived subject to the consistency requirement

$$\lambda + 2\delta = 3 \tag{13}$$

The weighting functions P_i $(i = 1, 2)$ are thus obtained as

$$P_1 = -(1 - \lambda)\xi \tag{14}$$

$$P_2 = (1 - \lambda)\xi \tag{15}$$

The resulting discrete equation is derived as follows in a domain with a uniform grid size:

$$\begin{aligned} &\left\{\left[\text{sgn}(m)\left(R_1 - \frac{u\tau}{h}R_2\right) - 6 + 4\lambda + \frac{\lambda}{3}R_2 - \frac{2u\tau}{h}R_1\right]\phi_{i+m}\right\}_{m=\{-1,1\}} \\ &\quad + \left[12 - 8\lambda + \frac{2(3-\lambda)}{3}R_2 + \frac{4u\tau}{h}R_1\right]\phi_i \\ &\quad = \left\{\left[\text{sgn}(m)\left(\frac{u\tau}{hR}R_2\right) + \frac{\lambda}{3R}R_2\right]f_{i+m}\right\}_{m=\{-1,1\}} + \left[\frac{2(3-\lambda)}{3R}R_2\right]f_i = 0 \end{aligned} \tag{16}$$

To present the discrete equation in a somewhat more compact form, the sign notation sgn($\circ$) shown above is employed.

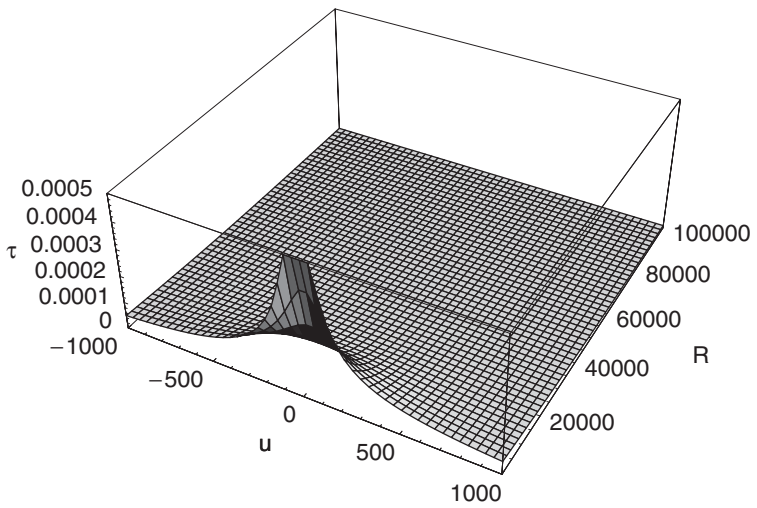

Figure 1. The plot of τ in the domain $-1000 < u < 1000,\ 10 < R < 100\,000$.

To complete the finite element model development, we need to determine τ shown in (6) and λ shown in (14) and (15). Our aim in determining them is to optimize the finite element model. To this end, the analytic solution, $\phi_{\text{exact}} = C_1 \exp(u/2\mu + (1/2\mu)\sqrt{u^2 + 4R\mu}) + C_2 \exp(u/2\mu - (1/2\mu)\sqrt{u^2 + 4R\mu})$, is substituted into the discrete equation (5), we can derive τ and λ as follows after some algebra:

$$\tau = \frac{h}{u}\left[\frac{R_1}{R_2} + \frac{\sinh(R_1)}{\cosh(R_1) - \cosh(\frac{1}{2}\sqrt{R_1^2 + R_2})}\right] \tag{17}$$

$$\lambda = \frac{3}{R_2}\left\{\frac{2(R_1^2 + 3R_2)}{(R_2 + 12)} + \frac{[R_2 \cosh(R_1) + 2R_1 \sinh(R_1)]}{(R_2 + 12)[\cosh(R_1) - \cosh(\frac{1}{2}\sqrt{R_1^2 + R_2})]}\right\} \tag{18}$$

In the above, C_1 and C_2 are two arbitrary constants. For clarity, we plot τ and λ in Figures 1 and 2 in terms of u and R, respectively. In the limiting case of zero reaction, τ in Equation (17) turns out to be that proposed by Hughes and Brooks [16]. It is also interesting to find that $\lim_{R \to 0} \lambda = 1$. This is desirable since $0 \leqslant \lambda \leqslant 1$ over the entire range of R.

Before proceeding with the next section, it is worth noting that use of τ and λ from Equations (17) and (18) renders a nodally exact solution to the model equation (3). Specification of these analytic convection and reaction coefficients forms the building block for the subsequent two-dimensional finite element model development.

4. TWO-DIMENSIONAL FINITE ELEMENT MODEL

The goal in developing the CDR finite element model in two dimensions is to retain the desirable feature of its one-dimensional model. For this reason, we exploit the tensor product

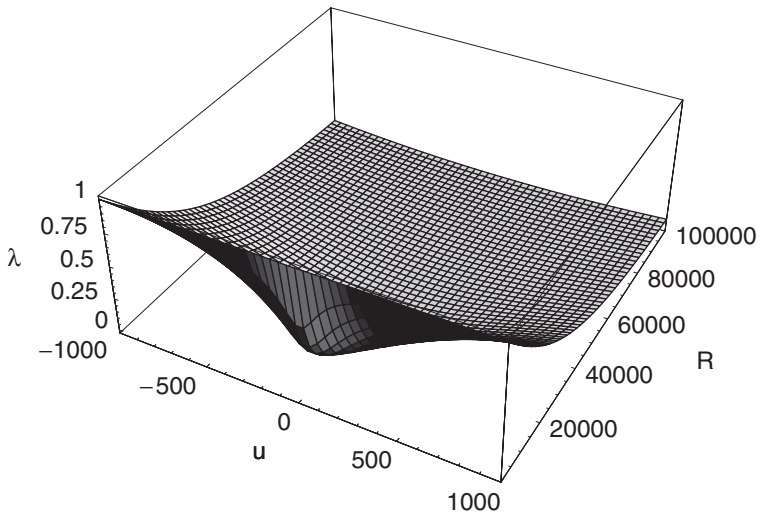

Figure 2. The plot of τ in the domain $-1000 < u < 1000,\ 10 < R < 100\,000$.

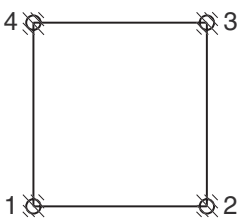

Figure 3. Numbering strategy for the bi-linear element.

operator

$$W_i = N_i + \tau_x u \frac{\partial N_i}{\partial x} + \tau_y v \frac{\partial N_i}{\partial y} + P_i \tag{19}$$

In the above, N_i $(i = 1 \sim 4)$ represents the bilinear shape functions. As a good stabilization means for the positive-valued reaction term, we introduce six coefficients $\lambda_x, \lambda_y, \delta_x, \delta_y, \tau_x$, and τ_y when constructing P_i. Referring to the element numbering schematic shown in Figure 3, $P_1 \sim P_4$ are expressed as

$$P_1 = P(-1, -1) \tag{20a}$$

$$P_2 = P(1, -1) \tag{20b}$$

$$P_3 = P(1, 1) \tag{20c}$$

$$P_4 = P(-1, 1) \tag{20d}$$

where $P(m,n)$ is defined as

$$\begin{aligned} P(m,n) = &-\frac{1}{4} + \frac{\delta_x\delta_y}{9} + \frac{\delta_y\lambda_x}{18} + \frac{\delta_x\lambda_y}{18} + \frac{\lambda_x\lambda_y}{36} \\ &+ \operatorname{sgn}(m)\xi\left(-\frac{1}{4} + \frac{\delta_x\delta_y}{3} - \frac{\delta_y\lambda_x}{6} + \frac{\delta_x\lambda_y}{6} - \frac{\lambda_x\lambda_y}{12}\right) \\ &+ \operatorname{sgn}(n)\eta\left(-\frac{1}{4} + \frac{\delta_x\delta_y}{3} + \frac{\delta_y\lambda_x}{6} - \frac{\delta_x\lambda_y}{6} - \frac{\lambda_x\lambda_y}{12}\right) \\ &+ \operatorname{sgn}(m)\operatorname{sgn}(n)\xi\eta\left(-\frac{1}{4} + \delta_x\delta_y - \frac{\delta_y\lambda_x}{2} - \frac{\delta_x\lambda_y}{2} + \frac{\lambda_x\lambda_y}{4}\right) \end{aligned} \tag{21}$$

Consistency is retained on condition that $2\delta_x + \lambda_x = 3$ and $2\delta_y + \lambda_y = 3$. Substitution of the above two consistency-satisfying constraints into Equation (21) enables us to rewrite $P(m,n)$ as

$$\begin{aligned} P(m,n) = &\operatorname{sgn}(m)\xi\left(\frac{1}{2} - \frac{\lambda_x}{2}\right) + \operatorname{sgn}(n)\eta\left(\frac{1}{2} - \frac{\lambda_y}{2}\right) \\ &+ \operatorname{sgn}(m)\operatorname{sgn}(n)\xi\eta\left(2 - \frac{3\lambda_x}{2} - \frac{3\lambda_y}{2} + \lambda_x\lambda_y\right) \end{aligned} \tag{22}$$

The consistent finite element equation is derived by multiplying the weighting function with every term shown in the differential equation (2). In this way, the discrete equation at a point (i,j) can be derived as

$$\begin{aligned} &\left[\left\{\left[\frac{\operatorname{sgn}(m)}{12}\left(\lambda_y R_{x1} - \frac{u\tau_x}{h}R_{x2}\right) - \frac{\lambda_y}{2} + \frac{\lambda_x\lambda_y}{3} - \frac{u\tau_x}{6h}R_{x1}\right.\right. \\ &\quad \left. - \operatorname{sgn}(m)\operatorname{sgn}(n)\frac{v\tau_y}{4k}R_{x1} + \frac{\lambda_x\lambda_y}{72}R_{x2}\right]k^2 \\ &\quad + \left[\frac{\operatorname{sgn}(n)}{12}\left(\lambda_x R_{y1} - \frac{v\tau_y}{k}R_{y2}\right) - \frac{\lambda_x}{2} + \frac{\lambda_x\lambda_y}{3} - \frac{v\tau_y}{6k}R_{y1}\right. \\ &\quad \left.\left. - \operatorname{sgn}(m)\operatorname{sgn}(n)\frac{u\tau_x}{4h}R_{y1} + \frac{\lambda_x\lambda_y}{72}R_{y2}\right]h^2\right\}\phi_{i+m,j+n}\Big]_{m=\{-1,1\},n=\{-1,1\}} \\ &\quad + \left[\left\{\left[\operatorname{sgn}(m)\left(\frac{1}{2}R_{x1} - \frac{\lambda_y}{6}R_{x1} - \frac{u\tau_x}{3h}R_{x2}\right) - 3 + 2\lambda_x + \lambda_y\right.\right. \\ &\quad \left. - \frac{2\lambda_x\lambda_y}{3} - \frac{2u\tau_x}{3h}R_{x1} + \frac{\lambda_x}{6}R_{x2}\right]k^2 \\ &\quad \left.\left. + \left[\lambda_x - \frac{2\lambda_x\lambda_y}{3} + \frac{v\tau_y}{3k}R_{y1} - \frac{\lambda_x\lambda_y}{18}R_{y2}\right]h^2\right\}\phi_{i+m,j}\right]_{m=\{-1,1\}} \end{aligned}$$

$$
\begin{aligned}
&+\left[\left\{\left[\operatorname{sgn}(n)\left(\frac{1}{2}R_{y1}-R_{y1}\frac{\lambda_x}{6}-\frac{v\tau_y}{3k}R_{y2}\right)-3+2\lambda_y+\lambda_x\right.\right.\right.\\
&\left.-\frac{2\lambda_x\lambda_y}{3}-\frac{2v\tau_y}{3k}R_{y1}+\frac{\lambda_y}{6}R_{y2}\right]h^2\\
&\left.+\left[\lambda_y-\frac{2\lambda_x\lambda_y}{3}+\frac{u\tau_x}{3h}R_{x1}-\frac{\lambda_x\lambda_y}{18}R_{x2}\right]k^2\right\}\phi_{i,j+n}\Bigg]_{n=\{-1,1\}}\\
&+\left[\left(\frac{1}{2}R_{x2}-\frac{\lambda_x}{6}R_{x2}-\frac{\lambda_y}{6}R_{x2}+\frac{\lambda_x\lambda_y}{18}R_{x2}+\frac{4u\tau_x}{3h}R_{x1}\right.\right.\\
&\left.+6-4\lambda_x-2\lambda_y+\frac{4\lambda_x\lambda_y}{3}\right)k^2\\
&+\left(\frac{1}{2}R_{y2}-\frac{\lambda_x}{6}R_{y2}-\frac{\lambda_y}{6}R_{y2}+\frac{\lambda_x\lambda_y}{18}R_{y2}+\frac{4v\tau_y}{3k}R_{y1}\right.\\
&\left.\left.+6-4\lambda_x-2\lambda_y+\frac{4\lambda_x\lambda_y}{3}\right)h^2\right]\phi_{i,j}\\
&=\left\{\frac{1}{12}\left[\left(\frac{-\operatorname{sgn}(m)u\tau_x}{h}R_{x2}+\frac{\lambda_x\lambda_y}{6}R_{x2}\right)\frac{k^2}{R}\right.\right.\\
&\left.\left.+\left(-\frac{\operatorname{sgn}(n)v\tau_y}{k}R_{y2}+\frac{\lambda_x\lambda_y}{6}R_{y2}\right)\frac{h^2}{R}\right]f_{i+m,j+n}\right\}_{m=\{-1,1\},n=\{-1,1\}}\\
&+\left\{\frac{1}{3}\left[\left(-\frac{\operatorname{sgn}(m)u\tau_x}{h}R_{x2}+\frac{\lambda_x}{2}R_{x2}\right)\frac{k^2}{R}-\frac{\lambda_x\lambda_y}{6}R_{y2}\frac{h^2}{R}\right]f_{i+m,j}\right\}_{m=\{-1,1\}}\\
&+\left\{\frac{1}{3}\left[\left(-\frac{\operatorname{sgn}(n)v\tau_y}{k}R_{y2}+\frac{\lambda_y}{2}R_{y2}\right)\frac{h^2}{R}-\frac{\lambda_x\lambda_y}{6}R_{x2}\frac{k^2}{R}\right]f_{i,j+n}\right\}_{n=\{-1,1\}}\\
&+\frac{1}{2}\left[\left(R_{x2}-\frac{\lambda_x}{3}R_{x2}-\frac{\lambda_y}{3}R_{x2}+\frac{\lambda_x\lambda_y}{9}R_{x2}\right)\frac{k^2}{R}\right.\\
&\left.+\left(R_{y2}-\frac{\lambda_x}{3}R_{y2}-\frac{\lambda_y}{3}R_{y2}+\frac{\lambda_x\lambda_y}{9}R_{y2}\right)\frac{h^2}{R}\right]f_{i,j}
\end{aligned}
\tag{23}
$$

Substituting the Taylor series expansion equations with respect to $\phi_{i,j}$ for $\phi_{i\pm1,j}, \phi_{i,j\pm1}$, and $\phi_{i\pm1,j\pm1}$ into the discrete equation (23) we obtain the following modified equation for (2) after a series of algebraic manipulations:

$$
\begin{aligned}
&u\phi_x+v\phi_y-\mu(\phi_{xx}+\phi_{yy})+R\phi-f\\
&\quad=Ru\tau_x\phi_x+Rv\tau_y\phi_y+uv(\tau_x+\tau_y)\phi_{xy}\\
&\qquad+\left[2\mu(1-\lambda_x)+u^2\tau_x-\frac{\lambda_x h^2R}{6}\right]\phi_{xx}+\left[2\mu(1-\lambda_y)+v^2\tau_y-\frac{\lambda_y k^2R}{6}\right]\phi_{yy}
\end{aligned}
$$

$$
\begin{aligned}
&+\frac{h^2u}{6}(-1+\tau_xR)\phi_{xxx}+\frac{h^2v}{6}(-\lambda_x+\tau_yR)\phi_{xxy}\\
&+\frac{k^2u}{6}(-\lambda_y+\tau_xR)\phi_{xyy}+\frac{k^2v}{6}(-1+\tau_yR)\phi_{yyy}\\
&+\frac{h^2}{6}\left[\frac{\mu}{2}+\mu(1-\lambda_x)+\frac{u^2\tau_x}{2}-\frac{\lambda_xh^2R}{12}\right]\phi_{xxxx}\\
&+\frac{k^2}{6}\left[\frac{\mu}{2}+\mu(1-\lambda_y)+\frac{v^2\tau_y}{2}-\frac{\lambda_yk^2R}{12}\right]\phi_{yyyy}\\
&+\left(\frac{\lambda_xh^2\mu}{2}+\frac{\lambda_yk^2\mu}{2}-\frac{\lambda_x\lambda_yh^2\mu}{3}-\frac{\lambda_x\lambda_yk^2\mu}{3}\right.\\
&\left.+\frac{\tau_xh^2v^2}{6}+\frac{\tau_yk^2u^2}{6}-\frac{\lambda_x\lambda_yh^2k^2R}{36}\right)\phi_{xxyy}\\
&+\frac{h^2uv}{6}(\tau_x+\tau_y)\phi_{xxxy}+\frac{k^2uv}{6}(\tau_x+\tau_y)\phi_{xyyy}+\cdots
\end{aligned}
\tag{24}
$$

It is well known that the production of mixed derivative terms will distort the true transport profile and, thus, severely contaminate the solution. A way to alleviate this problem is to eliminate the three leading mixed derivative terms, namely, $uv(\tau_x+\tau_y)\phi_{xy}$, $(uvh^2(\tau_x+\tau_y)/6)\phi_{xxxy}$, and $(uvk^2(\tau_x+\tau_y)/6)\phi_{xyyy}$ shown in Equation (24). We further refine the afore-mentioned consistent Petrov–Galerkin finite element model to obtain its inconsistent counterparts by adding a term $T\phi_{xy}$ to cancel out these mixed derivatives from the following explicit artificial finite element model:

$$
\int\int W_i(\underline{u}\cdot\nabla\phi-\mu\nabla^2+R\phi)+T\phi_{xy}\,\mathrm{d}x\,\mathrm{d}y=\int\int W_i f(x,y)\,\mathrm{d}x\,\mathrm{d}y \tag{25}
$$

Substituting (19) into (25), we can derive the following modified equation that is free of the mixed derivative terms ϕ_{xy}, ϕ_{xxxy} and ϕ_{xyyy}. The evidence is given in the following modified equation:

$$
\begin{aligned}
&u\phi_x+v\phi_y-\mu(\phi_{xx}+\phi_{yy})+R\phi-f\\
&\quad=Ru\tau_x\phi_x+Rv\tau_y\phi_y\\
&\qquad+\left[2\mu(1-\lambda_x)+u^2\tau_x-\frac{\lambda_xh^2R}{6}\right]\phi_{xx}+\left[2\mu(1-\lambda_y)+v^2\tau_y-\frac{\lambda_yk^2R}{6}\right]\phi_{yy}\\
&\qquad+\frac{h^2u}{6}(-1+\tau_xR)\phi_{xxx}+\frac{h^2v}{6}(-\lambda_x+\tau_yR)\phi_{xxy}\\
&\qquad+\frac{k^2u}{6}(-\lambda_y+\tau_xR)\phi_{xyy}+\frac{k^2v}{6}(-1+\tau_yR)\phi_{yyy}\\
&\qquad+\frac{h^2}{6}\left[\frac{\mu}{2}+\mu(1-\lambda_x)+\frac{u^2\tau_x}{2}-\frac{\lambda_xh^2R}{12}\right]\phi_{xxxx}
\end{aligned}
$$

$$+\frac{k^2}{6}\left[\frac{\mu}{2}+\mu(1-\lambda_y)+\frac{v^2\tau_y}{2}-\frac{\lambda_y k^2 R}{12}\right]\phi_{yyyy}$$
$$+\left(\frac{\lambda_x h^2\mu}{2}+\frac{\lambda_y k^2\mu}{2}-\frac{\lambda_x\lambda_y h^2\mu}{3}-\frac{\lambda_x\lambda_y k^2\mu}{3}\right.$$
$$\left.+\frac{\tau_x h^2 v^2}{6}+\frac{\tau_y k^2 u^2}{6}-\frac{\lambda_x\lambda_y h^2 k^2 R}{36}\right)\phi_{xxyy}+\cdots \tag{26}$$

Note that the validity of the above equation is subject to the specification of T, shown in (25), as

$$T=uv(\tau_x+\tau_y) \tag{27}$$

In this context, the discrete finite element equation at an interior point (i,j) is expressed as

$$\left[\left\{\left[\boxed{\frac{\mathrm{sgn}(m)}{12}\left(\lambda_y R_{x1}-\frac{u\tau_x}{h}R_{x2}\right)-\frac{\lambda_y}{2}+\frac{\lambda_x\lambda_y}{3}-\frac{u\tau_x}{6h}R_{x1}+\frac{\lambda_x}{36}R_{x2}}\right.\right.\right.$$
$$\left.+\frac{(1-\lambda_x)(1-\lambda_y)-1}{72}R_{x2}\right]k^2$$
$$+\left[\boxed{\frac{\mathrm{sgn}(n)}{12}\left(\lambda_x R_{y1}-\frac{v\tau_y}{12k}R_{y2}\right)-\frac{\lambda_x}{2}+\frac{\lambda_x\lambda_y}{3}-\frac{v\tau_y}{6k}R_{y1}+\frac{\lambda_y}{36}R_{y2}}\right.$$
$$\left.\left.+\frac{(1-\lambda_x)(1-\lambda_y)-1}{72}R_{y2}\right]h^2\right\}\phi_{i+m,j+n}\Bigg]_{m=\{-1,1\},n=\{-1,1\}}$$
$$+\left[\left\{\left[\boxed{\mathrm{sgn}(m)\left(\frac{1}{2}R_{x1}-\frac{\lambda_y}{6}R_{x1}-\frac{u\tau_x}{3h}R_{x2}\right)-3+2\lambda_x+\lambda_y-\frac{2\lambda_x\lambda_y}{3}-\frac{2u\tau_x}{3h}R_{x1}}\right.\right.\right.$$
$$\left.\boxed{+\frac{\lambda_x}{9}R_{x2}}\right]k^2+\left[\lambda_x-\frac{2\lambda_x\lambda_y}{3}+\frac{v\tau_y}{3k}R_{y1}+\frac{\lambda_x(1-\lambda_y)}{18}R_{y2}\right]h^2\Bigg\}\phi_{i+m,j}\Bigg]_{m=\{-1,1\}}$$
$$+\left[\left\{\left[\boxed{\mathrm{sgn}(n)\left(\frac{1}{2}R_{y1}-R_{y1}\frac{\lambda_x}{6}-\frac{v\tau_y}{3k}R_{y2}\right)-3+2\lambda_y+\lambda_x-\frac{2\lambda_x\lambda_y}{3}-\frac{2v\tau_y}{3k}R_{y1}}\right.\right.\right.$$
$$\left.\boxed{+\frac{\lambda_y}{9}R_{y2}}\right]h^2+\left[\lambda_y-\frac{2\lambda_x\lambda_y}{3}+\frac{u\tau_x}{3h}R_{x1}+\frac{(1-\lambda_x)\lambda_y}{18}R_{x2}\right]k^2\Bigg\}\phi_{i,j+n}\Bigg]_{n=\{-1,1\}}$$

$$
\begin{aligned}
&+\left[\left(\frac{1}{2}R_{x2}-\frac{\lambda_x}{6}R_{x2}-\frac{\lambda_y}{6}R_{x2}+\frac{\lambda_x\lambda_y}{18}R_{x2}+\frac{4u\tau_x}{3h}R_{x1}\right.\right.\\
&\left.+6-4\lambda_x-2\lambda_y+\frac{4\lambda_x\lambda_y}{3}\right)k^2\\
&+\left(\frac{1}{2}R_{y2}-\frac{\lambda_x}{6}R_{y2}-\frac{\lambda_y}{6}R_{y2}+\frac{\lambda_x\lambda_y}{18}R_{y2}+\frac{4v\tau_y}{3k}R_{y1}\right.\\
&\left.\left.+6-4\lambda_x-2\lambda_y+\frac{4\lambda_x\lambda_y}{3}\right)h^2\right]\phi_{i,j}\\
&=\left\{\frac{1}{12}\left[\left(\frac{-\mathrm{sgn}(m)u\tau_x}{h}R_{x2}+\frac{\lambda_x\lambda_y}{6}R_{x2}\right)\frac{k^2}{R}\right.\right.\\
&\quad\left.\left.+\left(-\frac{\mathrm{sgn}(n)v\tau_y}{k}R_{y2}+\frac{\lambda_x\lambda_y}{6}R_{y2}\right)\frac{h^2}{R}\right]f_{i+m,j+n}\right\}_{m=\{-1,1\},n=\{-1,1\}}\\
&\quad+\left\{\frac{1}{3}\left[\left(-\frac{\mathrm{sgn}(m)u\tau_x}{h}R_{x2}+\frac{\lambda_x}{2}R_{x2}\right)\frac{k^2}{R}-\frac{\lambda_x\lambda_y}{6}R_{y2}\frac{h^2}{R}\right]f_{i+m,j}\right\}_{m=\{-1,1\}}\\
&\quad+\left\{\frac{1}{3}\left[\left(-\frac{\mathrm{sgn}(n)v\tau_y}{k}R_{y2}+\frac{\lambda_y}{2}R_{y2}\right)\frac{h^2}{R}-\frac{\lambda_x\lambda_y}{6}R_{x2}\frac{k^2}{R}\right]f_{i,j+n}\right\}_{n=\{-1,1\}}\\
&\quad+\frac{1}{2}\left[\left(R_{x2}-\frac{\lambda_x}{3}R_{x2}-\frac{\lambda_y}{3}R_{x2}+\frac{\lambda_x\lambda_y}{9}R_{x2}\right)\frac{k^2}{R}\right.\\
&\quad\left.+\left(R_{y2}-\frac{\lambda_x}{3}R_{y2}-\frac{\lambda_y}{3}R_{y2}+\frac{\lambda_x\lambda_y}{9}R_{y2}\right)\frac{h^2}{R}\right]f_{i,j}
\end{aligned}
\tag{28}
$$

Inspection of the above nine-point stencil discrete equation shows that terms $a_{i,j}$ with $i\neq j$ do not have negative values and that $a_{ii}>0$ under all circumstances. To develop a monotonicity-preserving finite element model, $\tau_x, \tau_y, \lambda_x$ and λ_y should be devised to obtain an irreducible diagonally dominant matrix equation based on the M-matrix theory [17]. Considering an M-matrix, the inverse of this matrix is, by definition, positive. Subject to this condition, solutions computed from the M-matrix finite element equation are, in theory, monotonic. By means of this theory, τ_x and τ_y can be derived as follows to render $a_{ii}>0$ and $a_{ij}<0$ $(i\neq j)$:

$$
\tau_x=\frac{\begin{vmatrix} f_1 & \dfrac{vh^2}{3k}R_{y1} \\ f_2 & \mathrm{sgn}(v)\left(-\dfrac{vh^2}{3k}R_{y2}\right)-\dfrac{2vh^2}{3k}R_{y1}\end{vmatrix}}{\begin{vmatrix} \mathrm{sgn}(u)\left(-\dfrac{uk^2}{3h}R_{x2}\right)-\dfrac{2uk^2}{3h}R_{x1} & \dfrac{vh^2}{3k}R_{y1} \\ \dfrac{uk^2}{3h}R_{x1} & \mathrm{sgn}(v)\left(-\dfrac{vh^2}{3k}R_{y2}\right)-\dfrac{2vh^2}{3k}R_{y1}\end{vmatrix}}
\tag{29a}
$$

$$\tau_y = \frac{\begin{vmatrix} \operatorname{sgn}(u)\left(-\dfrac{uk^2}{3k}R_{x2}\right) - \dfrac{2uk^2}{3h}R_{x1} & f_1 \\ \dfrac{uk^2}{3h}R_{x1} & f_2 \end{vmatrix}}{\begin{vmatrix} \operatorname{sgn}(u)\left(-\dfrac{uk^2}{3h}R_{x2}\right) - \dfrac{2uk^2}{3h}R_{x1} & \dfrac{vh^2}{3k}R_{y1} \\ \dfrac{uk^2}{3h}R_{x1} & \operatorname{sgn}(v)\left(-\dfrac{vh^2}{3k}R_{y2}\right) - \dfrac{2vh^2}{3k}R_{y1} \end{vmatrix}} \tag{29b}$$

where

$$f_1 = -\left[\frac{1}{2}\operatorname{sgn}(u)\left(R_{x1} - \frac{\lambda_y}{3}R_{x1}\right) - 3 + 2\lambda_x + \lambda_y - \frac{2\lambda_x\lambda_y}{3} + \frac{\lambda_x}{6}R_{x2}\right]k^2 - \left(\lambda_x - \frac{2\lambda_x\lambda_y}{3} - \frac{\lambda_x\lambda_y}{18}R_{y2}\right)h^2 \tag{30a}$$

$$f_2 = -\left[\frac{1}{2}\operatorname{sgn}(v)\left(R_{y1} - \frac{\lambda_x}{3}R_{y1}\right) - 3 + 2\lambda_y + \lambda_x - \frac{2\lambda_x\lambda_y}{3} + \frac{\lambda_y}{6}R_{y2}\right]h^2 - \left(\lambda_y - \frac{2\lambda_x\lambda_y}{3} - \frac{\lambda_x\lambda_y}{18}R_{x2}\right)k^2 \tag{30b}$$

The validity of τ_x and τ_y shown above is subject to λ_x and λ_y, which take the same form as that derived in the one-dimensional analysis. The reason for using the one-dimensional representation of λ_x and λ_y is that the finite element equation shown in the block of equation (28) is akin to the one-dimensional finite element equation. Considering the inconsistent finite element model, we find from (18) and (29) that solutions exhibiting the sharp profile form can be obtained in the flow. We will address this issue through examples considered later.

5. NUMERICAL RESULTS

As is usually the case when a scheme for solving the differential equation is presented, we needed to validate the scheme. For this purpose, we employed test problems which were amenable to analytic solutions. To make matters simple, we assumed that $\mu = 1$, $u = 1$, and $R = 2$ in the analysis of one-dimensional CDR equation, where $f = u\cos x + (\mu + R)\sin x$. Subject to the Dirichlet-type boundary condition, the exact solution to the inhomogeneous CDR equation was derived as follows:

$$\phi_{\text{exact}} = \sin x \tag{31}$$

Uniform grids were overlaid on the region $0 \leqslant x \leqslant 1$. The finite element result plotted in Figure 4 and the L_2-error norm (1.322×10^{-7}) show good agreement with the exact solution, thus demonstrating the applicability of the proposed scheme to solving the inhomogeneous CDR equation.

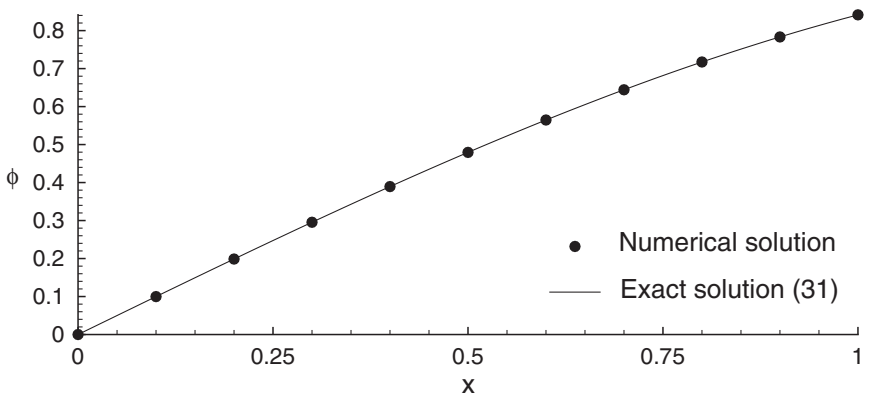

Figure 4. The comparison of exact and numerical solutions for the problem with a smooth solution.

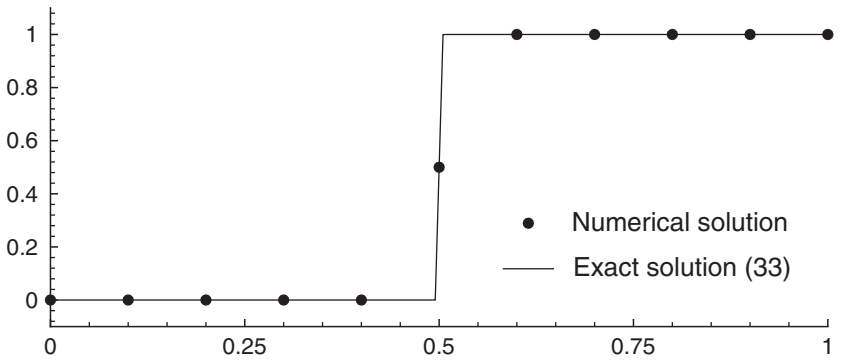

Figure 5. The comparison of exact and numerical solutions for the problem with a sharp gradient solution.

To further verify that the scheme is applicable to problems containing the discontinuous source term, we considered the case in which

$$f = \begin{cases} 0, & x < \dfrac{1}{2} \\ R, & x \geqslant \dfrac{1}{2} \end{cases} \tag{32}$$

Subject to the boundary conditions $\phi(x=0)=0$ and $\phi(x=1)=1$, the exact solution takes the following form:

$$\phi = \begin{cases} \dfrac{1}{2}\dfrac{\sinh(\alpha x)}{\sinh(\alpha/2)}, & x < \dfrac{1}{2} \\ 1 - \dfrac{1}{2}\dfrac{\sinh(\alpha(1-x))}{\sinh(\alpha/2)}, & x > \dfrac{1}{2} \end{cases} \tag{33}$$

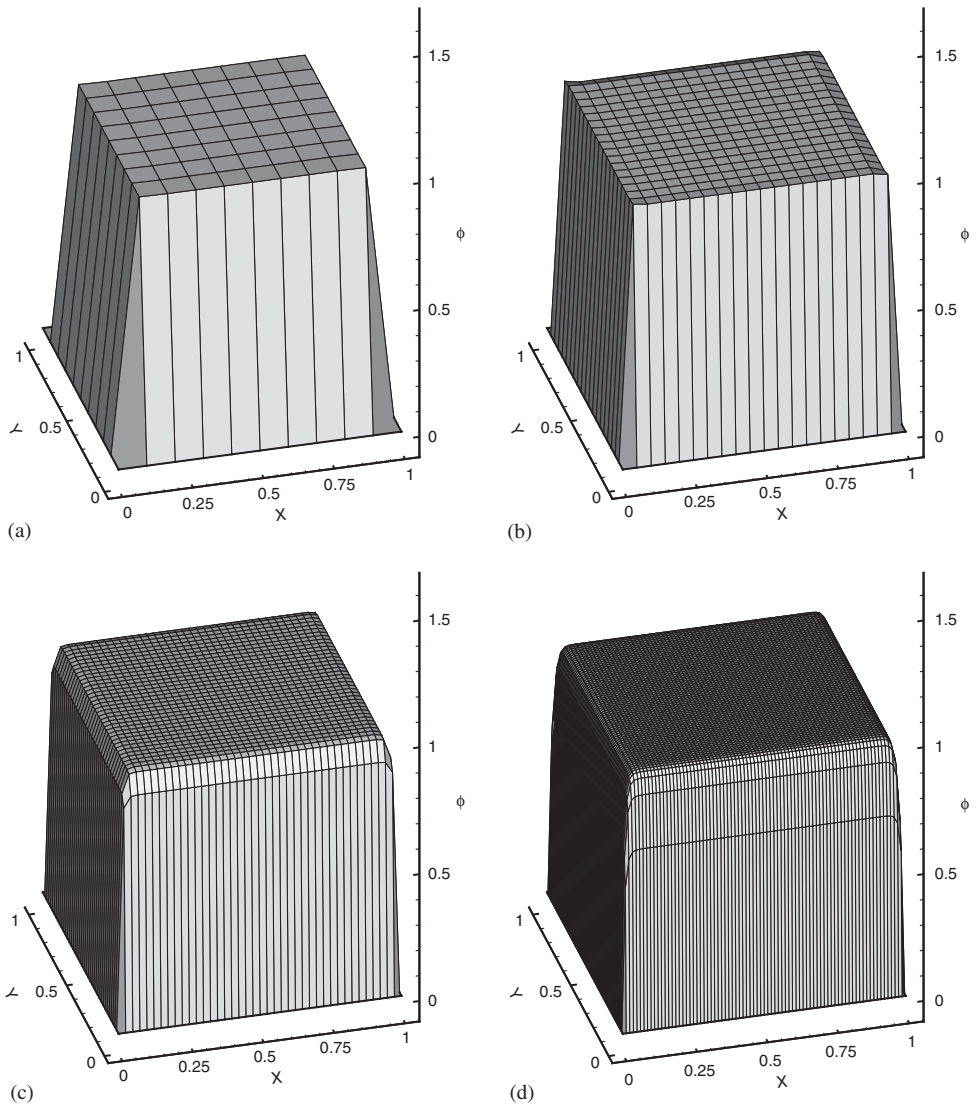

Figure 6. The plots of ϕ for the first two-dimensional test case at: (a) $\Delta x = \Delta y = \frac{1}{10}$; (b) $\Delta x = \Delta y = \frac{1}{20}$; (c) $\Delta x = \Delta y = \frac{1}{40}$; and (d) $\Delta x = \Delta y = \frac{1}{80}$.

where $\alpha = (\sqrt{R/\mu})$. In this case, we considered $\mu = 1$, $u = 0$, $R = 10^4$ and $h = \frac{1}{10}$. Figure 5 shows the exact solution in full line and numerical solution shown in symbols. As evident from the L_2-error norm 9.2046×10^{-8}, good agreement between the two solutions was obtained.

We proceeded to verify the applicability of the proposed two-dimensional finite element model. The first validation test case involves variable coefficients: $u = \sin \pi x$, $v = \sin \pi y$, $\mu = xy$, and $R = xy$. Subject to $f = (1 + 2\pi^2)xy \sin \pi x \sin \pi y + \pi(\cos \pi x + \cos \pi y)$, the exact smooth solution can be easily derived as $\phi = \sin \pi x \sin \pi y$. In this test, a series of

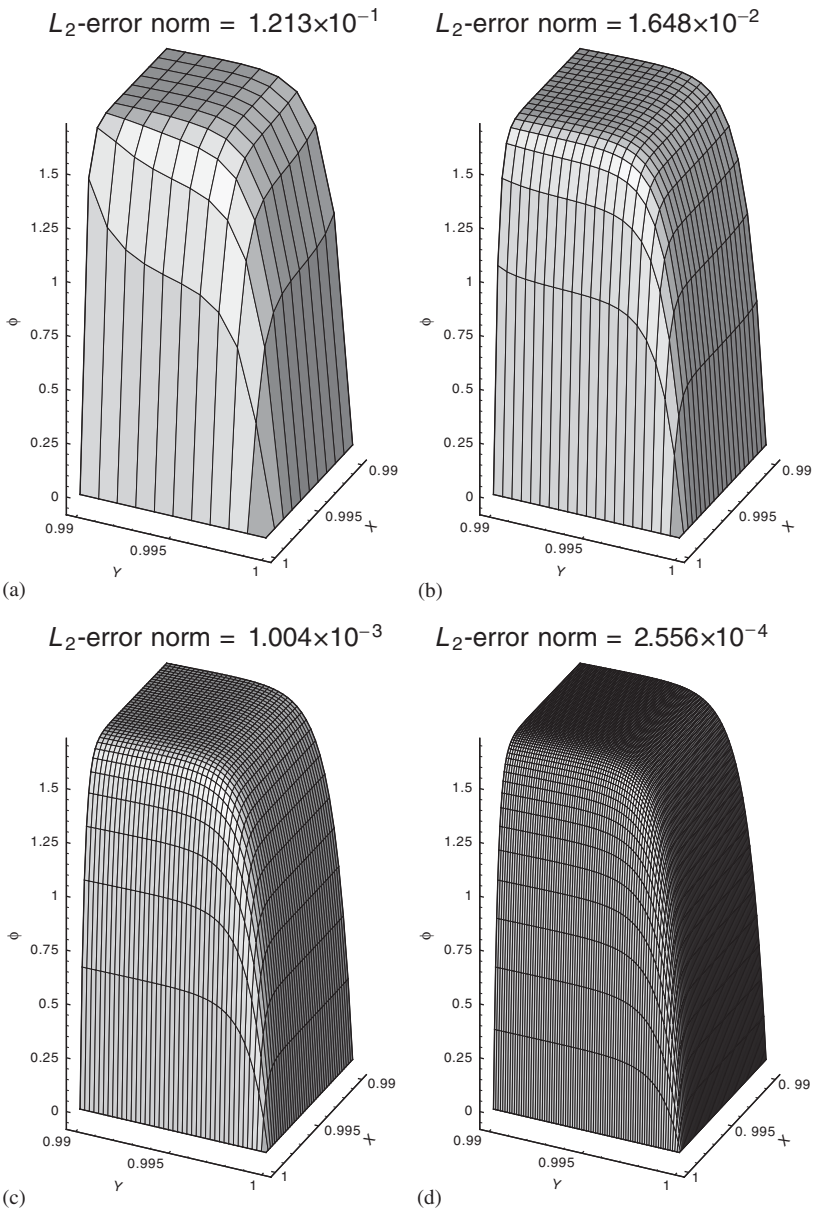

Figure 7. The plots of ϕ for the second two-dimensional test case, given in (34), computed at: (a) $\Delta x = \Delta y = \frac{1}{10}$; (b) $\Delta x = \Delta y = \frac{1}{20}$; (c) $\Delta x = \Delta y = \frac{1}{40}$; (d) $\Delta x = \Delta y = \frac{1}{80}$.

continuously refined uniform grids has been considered. The L_2-error norms are obtained as 0.4793×10^{-2}, 0.3099×10^{-2}, 0.1422×10^{-2} and 0.5320×10^{-3} for grids with the resolutions of 11×11, 21×21, 41×11 and 81×81, respectively.

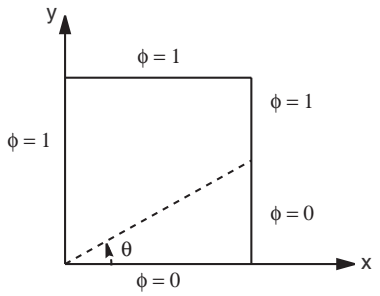

Figure 8. Schematic of the skew advection problem.

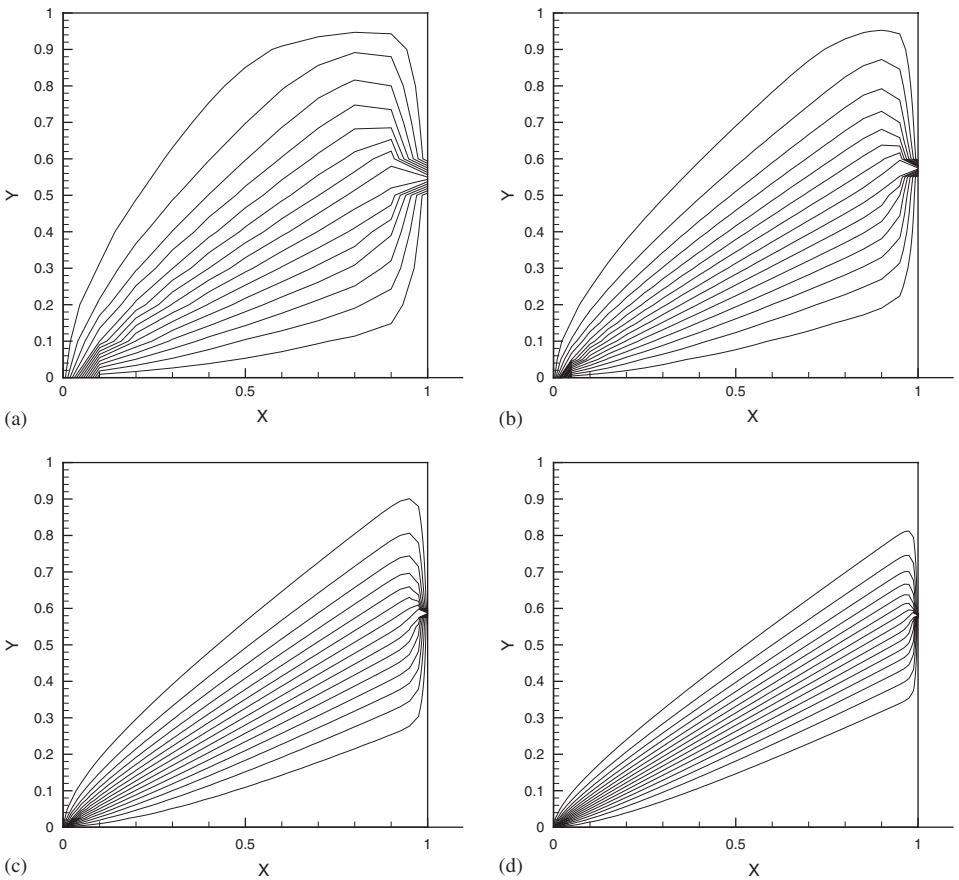

Figure 9. The computed contour profiles of ϕ computed at different grids: (a) 11×11; (b) 21×21; (c) 41×41; and (d) 81×81.

The second case, considered previously by Codina [14], involves $f = 1$, $R = 1$, $\mu = 10^{-4}$ and $\underline{u} = (10^{-4}\cos(\pi/3),\ 10^{-4}\sin(\pi/3))$. Subject to the Dirichlet-type boundary condition ϕ ($\bar{x} \in \partial\Omega$), simulations were performed on uniform grids with different resolutions of $\Delta x = \Delta y =$

$1/10, 1/20, 1/40$ and $1/80$. Finite element results shown in Figure 6 reveal that sharp profiles of ϕ could be captured without incurring oscillations.

Another problem [18] was chosen to show the ability of the proposed finite element model to obtain oscillation-free solutions in a domain containing sharp layers. With $\mu = 10^{-8}$, $\underline{u} = (2, 3)$, and $R = 1$, the source term f was properly chosen so as to render the exact solution given below

$$\phi(x, y) = 2y^2 \sin x \left[1 - \exp\left(\frac{-2(1-x)}{\mu}\right)\right]\left[1 - \exp\left(\frac{-(1-y)}{\mu}\right)\right] \tag{34}$$

In the domain $0.99 \leqslant x \leqslant 1.0$, $0.99 \leqslant y \leqslant 1.0$, finite element solutions were sought at four uniform gird sizes: $\Delta x = \Delta y = 10^{-3}/10, 10^{-3}/20, 10^{-3}/40$ and $10^{-3}/80$. As in the previous test, the boundary layer profiles shown in Figure 7 were obtained without incurring oscillations.

For the sake of completeness, we also apply the presently developed monotonic CDR model to solve for the skew advection problem [19], which has been frequently chosen to benchmark the discontinuity-capturing convection–diffusion models. In Figure 8, the dashed line, with the angle of $\theta(= \tan^{-1} v/u = \pi/6)$, divides the unit cavity into two parts. The flow condition under investigation is that with $\mu = 2 \times 10^{-4}$ and $(u, v) = (\sqrt{3}/2, \frac{1}{2})$. It is seen from Figure 9 that no oscillation has been observed near the dividing line for each test grid. This demonstrates the ability of the proposed model to resolve the interior sharp layer.

6. CONCLUDING REMARKS

We have presented in this paper the Petrov–Galerkin finite element model for solving the convection–diffusion-reaction equation in two dimensions. Our aim is to retain stability without reducing accuracy. To achieve this goal, we add a term to make the consistent finite element model into its inconsistent counterparts so as to eliminate three leading mixed derivatives. Good agreement with the smoothly varying exact solution has been obtained, thus verifying the applicability of the proposed finite element model. We have also extended the finite element model based on the M-matrix theory and applied it to solve a problem involving large gradients. Computations have demonstrated the model's ability to capture sharply varying profiles near the boundary as well as in the flow interior.

ACKNOWLEDGEMENTS

Financial support from the National Science Council of the Republic of China under Grant NSC88-2611-E-002-025 is acknowledged.

REFERENCES

1. Ilinca F, Pelletier D. Positivity preservation and adaptive solution for the k–ε model of turbulence. *AIAA Journal* 1988; **36**(1):44–50.
2. Crochet MJ, Davies AT, Walters K. *Numerical Simulation of Non-Newtonian Flow*. Elsevier: New York, 1984.
3. Leboucher L. Monotone scheme and boundary conditions for finite volume simulation of magnetohydrodynamic internal flows at high Hartmann number. *Journal of Computational Physics* 1999; **150**:181–198.
4. Harari I, Hughes TJR. Finite element methods for the Helmholtz equation in an exterior domain: model problems. *Computer Methods in Applied Mechanics and Engineering* 1991; **87**:59–96.

5. Ataie-Ashtini B, Lockington DA, Volker RE. Numerical correction of finite difference solution of the advection–dispersion equation with reaction. *Journal of Contaminant Hydrology* 1996; **23**:149–156.
6. Hossain MA. Modeling advective–dispersive transport with reaction: An accurate explicit finite difference model. *Applied Mathematics and Computation* 1999; **102**:101–108.
7. Hossain MA, Young DR. On Galerkin models for transport in groundwater. *Applied Mathematics and Computation* 1999; **100**:249–263.
8. Harari I, Hughes TJR. Stabilized finite element methods for steady advection–diffusion with production. *Computer Methods in Applied Mechanics and Engineering* 1994; **155**:165–191.
9. Idelsohn S, Nigro N, Storti M, Buscaglia G. A Petrov–Galerkin formulation for advection–reaction-diffusion problems. *Computer Methods in Applied Mechanics and Engineering* 1996; **136**:27–46.
10. Uri M Ascher, Robert MM Mattheij, Robert D Russell. *Numerical Solution of Boundary Value Problems for Ordinary Differential Equations*. Prentice-Hall: New Jersey, 1998; 454–456.
11. Doolan EP, Miller JJH, Schilders WHA. *Uniform Numerical Methods for Problems with Initial and Boundary Layers*. Boole Press: Dubin, 1980.
12. Tezdugar T, Park Y. Discontinuity capturing finite element formulations for nonlinear convection–diffusion-reaction equations. *Computer Methods in Applied Mechanics and Engineering* 1986; **59**:307–325.
13. Codina R. A chock-capturing anisotropic diffusion for the finite element solution of the diffusion–convection-reaction equation. *Finite Element in Fluids*, *New trends and Applications Part 1*, Morgan K. (ed.), Pineridge: Swansea, 1993; 67–75.
14. Codina R. Comparison of some finite element methods for solving the diffusion–convection–reaction equation. *Computer Methods in Applied Mechanics and Engineering* 1998; **156**:185–210.
15. Warming RF, Hyette BJ. The modified equation approach to the stability and accuracy analysis of finite-difference methods. *Journal of Computational Physics* 1974; **14**:159–179.
16. Hughes TJR, Brooks AN. A multi-dimensional upwind scheme with no crosswind diffusion. In *Finite Element Methods for Convection Dominated Flows*, Hughes TJR (ed.), AMD 34: ASME: New York, 1979; 19–35.
17. Meis T, Marcowitz U. Numerical solution of partial differential equations. In *Applied Mathematical Science*. John F, Sirovich L, La Salle JP (eds). Springer: Berlin, 1981; 32.
18. Linß T, Stynes M. Numerical methods on shishkin meshes for linear convection–diffusion problems. *Computer Methods in Applied Mechanics and Engineering* 2001; **190**:3527–3542.
19. Griffiths DF, Mitchell AR. In *Finite Element for Convection Dominated Flows*, Hughes TJR (ed.), in AMD 34. ASME: New York, 1979; 91–104.

